PASJ: Publ. Astron. Soc. Japan **56**, 225–234, 2004 February 25

Performance of Subaru Cassegrain Adaptive Optics System

Hideki TAKAMI,[1] Naruhisa TAKATO,[1] Yutaka HAYANO,[2] Masanori IYE,[2,3] Shin OYA,[1]
Yukiko KAMATA,[4] Tomio KANZAWA,[1] Yosuke MINOWA,[1,5] Masashi OTSUBO,[4] Koji NAKASHIMA,[6]
Wolfgang GAESSLER,[7] and David SAINT-JACQUES[8]

[1]*Subaru Telescope, National Astronomical Observatory of Japan, North A'Ohoku Place, Hilo, HI96720, USA*
takami@subaru.naoj.org

[2]*National Astronomical Observatory, Mitaka, Tokyo 181-8588*
iye@optik.mtk.nao.ac.jp

[3]*Department of Astronomy, Graduate University for Advanced Studies, Hayama, Kanagawa 240-0193*

[4]*Advanced Technology Center, National Astronomical Observatory, Mitaka, Tokyo 181-8588*

[5]*Department of Astronomy, The University of Tokyo, Bunkyo, Tokyo 113-0033*

[6]*Hitachi Software Engineering Co. Ltd., Higashi Shinagawa 4-12-7, Tokyo 140-0002*

[7]*Max-Plank Institut für Astronomie, Königstuhl 17, 69117 Heidelberg, Germany*

[8]*Department de physique, Université de Montréal, Montréal (Québec) H3C 3J7, Canada*

(Received 2003 June 27; accepted 2003 November 7)

Abstract

The design and performance of the Cassegrain Adaptive Optics (AO) system for the 8.2 m Subaru Telescope are reported. The system is based on a curvature wavefront sensor with 36 photon-counting avalanche photodiode modules and a bimorph wavefront correcting deformable mirror with 36 driving electrodes. The engineering first light of the AO system took place in 2000 December. The AO system has been in service since 2002 April for two open-use instruments, an infrared camera and spectrograph and a coronagraph imager with adaptive optics. The Strehl ratio in the K-band is around 0.3 for bright guide stars under $0\farcs4$ K-band seeing condition. The control loop performs with 2060 corrections per second. High sensitivity of the wavefront sensor allows significant improvement in the image quality, even for faint guide stars down to $R = 18$ mag. The FWHM of stellar images in a globular cluster was measured to derive an estimation of the isoplanatic angle and was found nearly constant out to $30''$ from the guide star, indicating that the height of the effective turbulent layer of that particular night was less than 1.8 km. The on-going upgrade plans for a fivefold increase in the number of control elements and for the installation of a laser guide AO system are described.

Key words: atmospheric effects — infrared: general — instrumentation: adaptive optics — instrumentation: high angular resolution — telescopes

1. Introduction

Atmospheric turbulence disturbs the incoming wavefront from astronomical sources and significantly degrades the image quality obtained by ground-based telescopes. For instance, whereas the diffraction limited resolution of the 8.2 m Subaru Telescope is $0\farcs02$ in the visible R-band, or $0\farcs06$ in the near infrared K-band, the best image sizes actually achieved without adaptive optics are $0\farcs3$ in the R-band with Suprime-Cam (Miyazaki et al. 2002) and $0\farcs2$ in the K-band with the CISCO (Motohara et al. 2002). The median seeing size evaluated by the acquisition/guide camera of Subaru Telescope is $0\farcs65$ (Miyashita et al. 2003; Iye et al. 2003). An adaptive optics (AO) system, as originally proposed by Babcock (1953), can overcome this practical limitation due to the turbulent atmosphere by compensating the time varying distorted wavefront in real time using a deformable mirror.

Basic studies toward the realization of an astronomical adaptive optics system in Japan began in the early 90's. Conceptual-design studies and some experimental developments for the construction of an adaptive optics system for the Cassegrain focus of the Subaru Telescope were made (Takato et al. 1994; Otsubo et al. 1995) with a series of grants in aid for scientific research. The system design was optimized to maximize its performance at near-infrared wavelengths with a relatively small number of control elements, i.e., 36. The primary reason for adopting a low-order AO system with a very sensitive wavefront sensor, rather than a high-order AO system, was its wider sky coverage for astronomical observations (Roddier et al. 1991). Early results of design studies and the development of a holographic turbulent simulator (Takami et al. 1994; Takami, Iye 1994; Otsubo et al. 1997) and progress reports of construction and early results of test observations (Takami et al. 1998, 2001, 2003a, 2003b) can be traced back in the literature.

2. System Overview

The Subaru Cassegrain AO unit was designed for installation on an optical bench placed about 330 mm above the Cassegrain focus, inside the auxiliary optics section. The auxiliary optics section with an inner diameter of 1.6 m and a total thickness of 800 mm houses three layers from bottom to top: the acquisition and guider layer, the adaptive optics layer, and the calibration

Table 1. Specifications of the Subaru Cassegrain adaptive optics system.

Spectral coverage	1–5 μm for compensation, 0.5–20 μm for transmission
Wavefront sensor	Wavefront curvature sensor with 36 photon counting APDs
Deformable mirror	Bimorph mirror with 36 control electrodes
Beam diameter	61 mm
Focal length	720 mm
Focal ratio	$F/12.4$
Field of view	$2'$
Tip/tilt mirror stroke*	$\pm 2''$
Control bandwidth	$\geq$ 100 Hz, 2060–2100 corrections s^{-1}

* Available for dithering the beam without moving the telescope for observations that do not require high precision photometry.

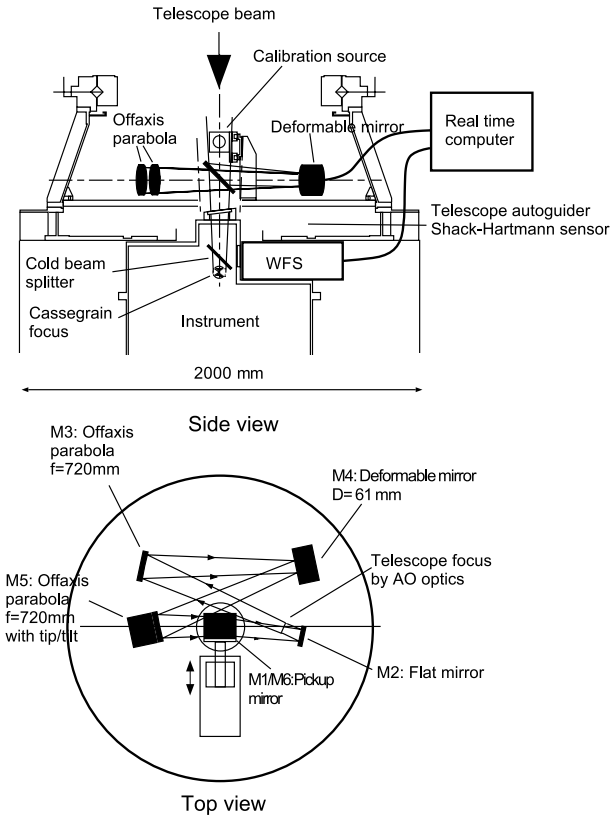

Fig. 1. Layout of the Subaru AO system. Top: Side view of the Cassegrain focus unit. The wavefront sensor is directly mounted on the science instrument. Bottom: Top view of the AO optics. The optics consist of a pair of off-axis paraboloid mirrors providing a $2'$ wide field of view by cancellation of coma and astigmatism aberrations.

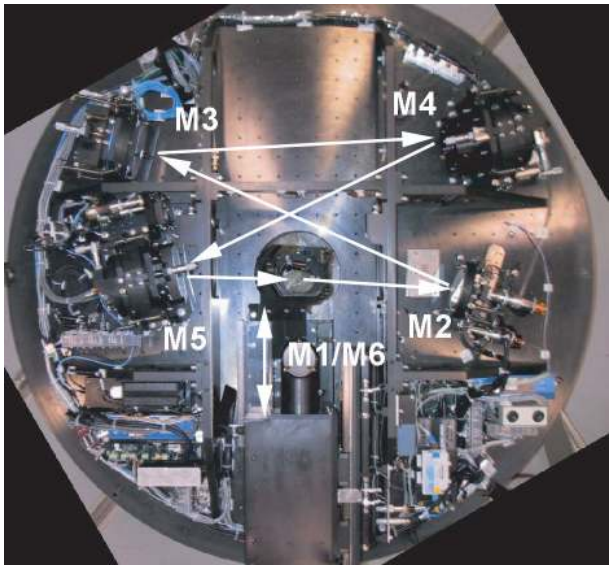

Fig. 2. Top view of the main optics bench of the AO system. M1: pick up flat mirror, M2: folding flat mirror, M3: off-axis parabola, M4: deformable mirror, M5: off-axis parabola on a tip-tilt mount, and M6: returning flat mirror.

unit layer (cf. figures 1 and 2). The wavefront sensor unit is attached directly to the scientific instrument to minimize the relative mechanical flexure between the two units.

The specifications of the AO system are listed in table 1. A pick-up mirror inserted in the telescope beam 460 mm in front of the Cassegrain focus directs the beam to the AO optics. The AO optics is composed of a combination of two off-axis paraboloid mirrors with identical focal length (720 mm), off-axis angle (24°), and diameter (150 mm). This layout enables the cancellation of coma and astigmatism aberrations, providing a field of view larger than $2'$. The deformable mirror is placed in the collimated beam between these two mirrors. The second paraboloid mirror is also used for a tip-tilt correction. The wavefront corrected beam is finally fed back by means of a flat mirror mounted on the backside of the pick-up mirror to the original Cassegrain focus. By retracting this unit of mirrors, the beam goes directly to the scientific instrument without changing the focal position or the focal ratio.

2.1. *Wavefront Curvature Sensor*

The wavefront sensor (WFS) is based on curvature measurement of atmospheric turbulence (Roddier, Roddier 1989; Graves et al. 1994). The wavefront curvature distribution in the entrance pupil is converted to a distribution of light intensity modulation at two positions before and after the pupil plane (cf. figure 3). The actual switching between the two planes can be achieved by a vibrating mirror placed at the telescope focus.

Figures 4 and 5 show the optical layout of the wavefront sensor and an actual photograph of the assembled unit. The

Table 2. Parameters of the wavefront sensor optics.

Component	Focal length (mm)	Diameter (mm)	Beam diameter (mm)
Collimator lens	65.13	25	5.20
Focusing lens	351.71	30	5.20
Concave mirror	290.00	30	4.33

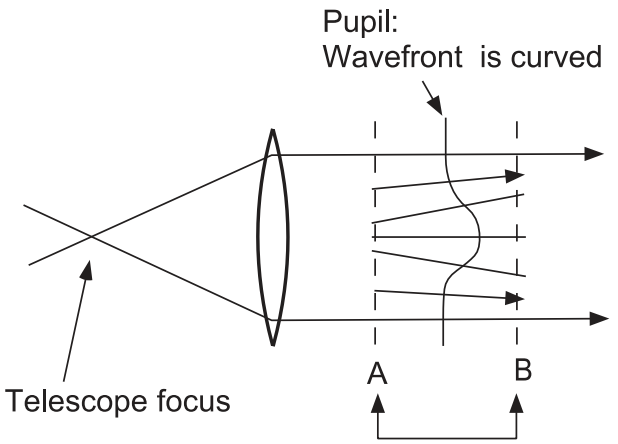

Fig. 3. Principle of the curvature wavefront sensor. The wavefront curvature distribution can be evaluated by measuring the non-uniform illumination at two positions, A and B, before and after the pupil plane. A vibrating mirror at the telescope focus provides the modulation of sampled positions and the wavefront sensor (figure 4) measures synchronously the modulated signal.

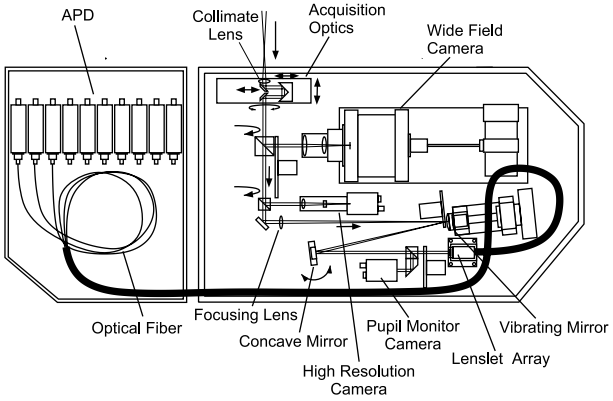

Fig. 4. Layout of the wavefront sensor.

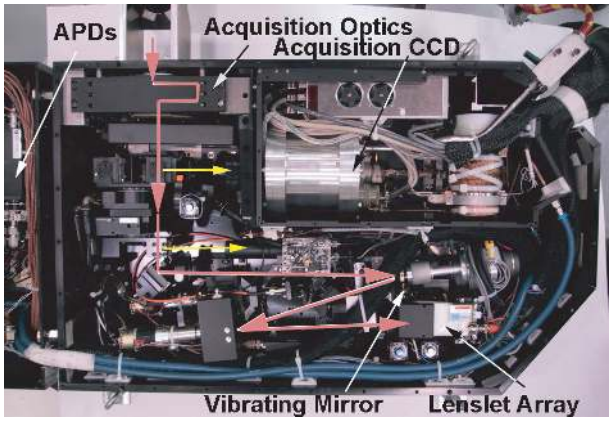

Fig. 5. Photograph of the wavefront sensor.

modulated light intensity signal is sampled at each sub-aperture of a microlens array and fed through optical fibers to photon-counting avalanche photodiode (APD) modules. The current Subaru AO system has 36 sub-apertures, the same number as the Hokupa'a AO system developed by the University of Hawaii group (Graves et al. 2000), but was designed independently. Table 2 gives the optical parameters of the Subaru WFS.

For low order compensation, a curvature-sensor AO system combined with a bimorph deformable mirror have the advantage of providing a higher Strehl ratio compared with a Shack–Hartmann sensor AO systems of corresponding number of control elements (Roddier 1998). Another benefit of this type of sensor is that one can use photon-counting avalanche photodiodes without readout noise, while for Shack–Hartmann sensors the readout noise of CCD detector becomes the dominant error source for faint guide stars. Curvature-sensor AO systems provide point spread functions with smoother wings in contrast to Shack–Hartmann-sensor AO systems that often show waffle-mode artifacts (Bloemhof et al. 2000).

The optical light is directed by a dichroic mirror towards the wavefront sensor. The wavefront sensor unit is attached to a science instrument, which is mounted on the Cassegrain instrument de-rotator. The wavefront sensor is equipped with guide star acquisition optics that can be driven on an (r, θ) mount to introduce any guide star within a $2'$ radius to the center of the wavefront sensor field of view. The acquisition of the guide star can be performed semi-automatically by communicating the coordinates read on the science camera to the acquisition optics drive system. The effective focal ratio of the wavefront sensor optics is converted to $F/66.8$ at the vibrating mirror. The vibrating mirror provides a modulation up to the maximum curvature of $\pm 0.0093\,\mathrm{mm}^{-1}$. The optimum amplitude of focal modulation depends on the seeing. Modulation at 60–80% of the maximum stroke is adopted for a seeing condition of $0.''5$ or better, while 20% modulation is used for seeing of about $1''$.

The field of view of the wavefront sensor, limited by the size of the optical fibers and the diameter of the vibrating mirror, is $5''$. For faint guide stars, one can reduce the field of view by using an iris stop of variable aperture size placed in front of the vibrating mirror to reduce the sky background. For bright guide stars, one of 10 neutral-density filters can be used to attenuate the light. Stars as bright as $R = 10.5$ can be used as a guide star.

A $1\mathrm{k} \times 1\mathrm{k}$ cooled CCD (EEV CCD47-20) camera covering a $20''$ field is used to monitor the guide star (cf. Wide Field Camera in figure 4).

The beam incident on the wavefront sensor is collimated and

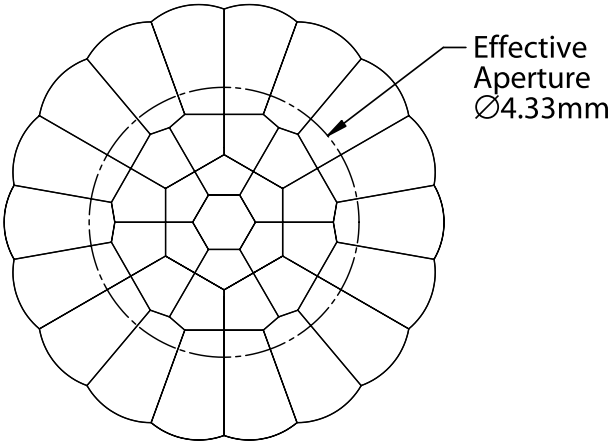

Fig. 6. Geometry of the lens array of the wavefront sensor. The plastic lens array was produced using a diamond-machined metal mold. The inner 18 lenses measure wavefront curvature while the outermost 18 lenslets measure wavefront tilt.

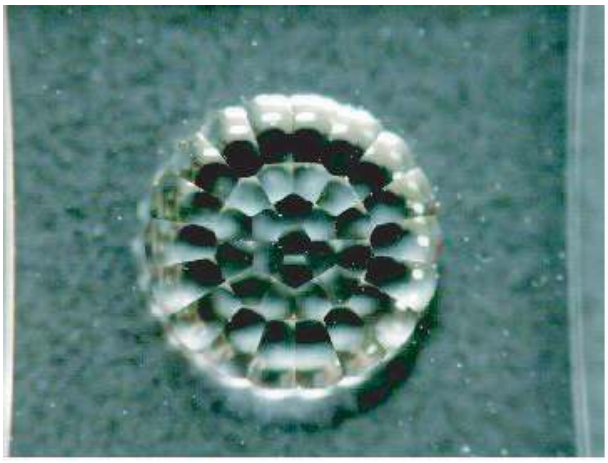

Fig. 7. The 36-elements molded plastic lenslet array. The effective aperture size is 4.33 mm and the total lens diameter is 6.9 mm.

illuminates a lenslet array placed at the pupil plane to divide the beam into 36 sub-apertures. The lenslet array we use is a plastic molded lens with an effective diameter of 4.33 mm with sub-aperture sizes of individual lenslet ranging from 0.7 to 2.2 mm (cf. figures 6 and 7). The plastic lens was fabricated by replication from a precisely diamond-machined copper mold. The innermost 6 lenslets and intermediate 12 lenslets measure the local wavefront curvature, whereas the outermost 18 lenslet arrays measure the wavefront slope at the edge of the telescope aperture.

Each lenslet feeds light into an optical fiber of 200 μm core diameter, twice the size of those used for other curvature sensor AO systems. The output light from the 200 μm fiber is refocused by an aspheric glass mold lens onto a Perkin Elmer APD of 200 μm diameter. The 36 APD modules were tested to have 70% photon detection efficiency (Takami et al. 1998; Gaessler et al. 2002).

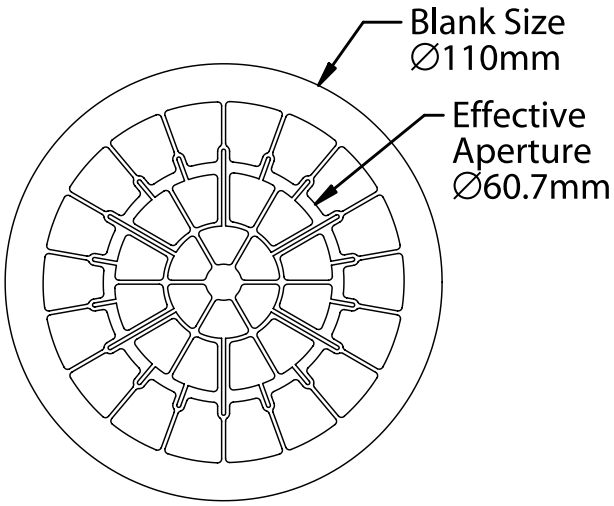

Fig. 8. Optimal electrode pattern of the bimorph deformable mirror with a useful aperture of 61 mm, and an overall diameter of 110 mm. The measured resonant frequency is 550 Hz.

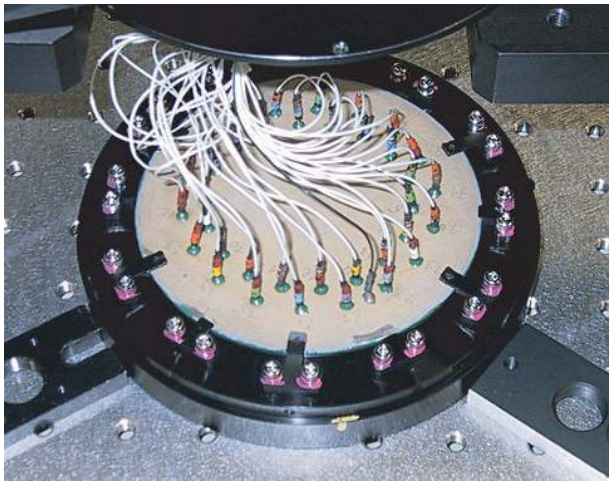

Fig. 9. Back view of the bimorph deformable mirror.

2.2. *Deformable Mirror*

Deformable mirror manufactured by CILAS is piezoelectrically driven by 36 bimorph control electrodes designed at NAOJ (cf. figures 8 and 9). The blank size of the mirror is 110 mm in diameter and 2.2 mm in thickness, while the effective diameter used for compensating the wavefront is 61 mm. The resonant frequency of this mirror supported at 6 peripheral points is 550 Hz. Although this is lower than the calculated frequency of 1.2 kHz of the mirror supported at its entire edge, it is still high enough for our targeted control bandwidth of 100 Hz and there is no degradation of the dynamic response.

2.3. *Calibration Light Source Unit*

A retractable calibration light source unit providing $F/12.4$ visible (650 nm) and infrared (1.55 μm) beams to produce a diffraction-limited image can be inserted in the optical path. An optical phase plate that generates wavefront turbulence

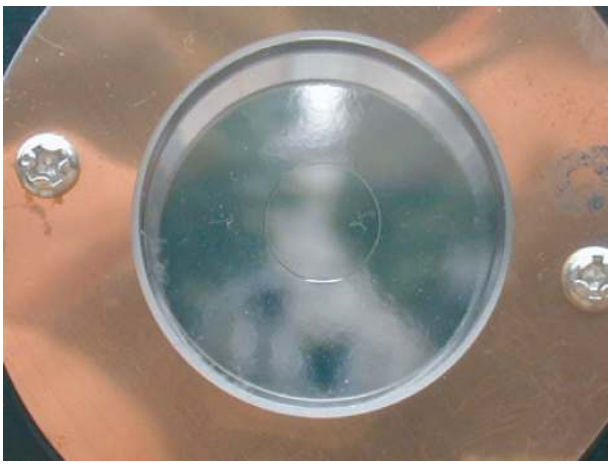

Fig. 10. Optical phase plate generating Kolmogorov turbulence corresponding to a 0.″3 image at K-band. The phase modulation is imprinted on the annular region. This plate is inserted in the optical path of a calibration visible/infrared light source. By rotating this plate one can produce a time-varying stellar image disturbed by simulated atmospheric turbulence.

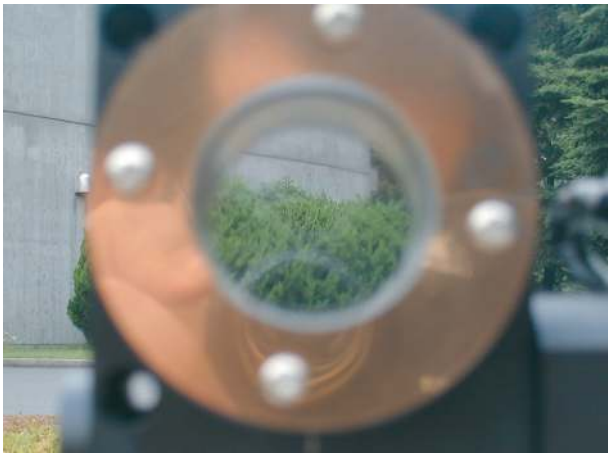

Fig. 11. Image through the optical phase plate shows its blurring effect in the annular region.

simulating Kolmogorov statistics which produces a stellar image of about 0.″3 in the H-band, is also mounted in front of the calibration light source (cf. figures 10 and 11). By rotating the phase plate, we can generate a time-varying wavefront to test the closed-loop performance during the daytime. The phase plate was also made of plastic replicated from a copper mold that was diamond-machined based on computer-generated wavefront turbulence data.

2.4. Control Computer

Figure 12 shows a control diagram of the Subaru adaptive optics system. We use two computer systems for controlling the AO system. One is a real-time control system (RTS) for the AO system itself, and the other is an instrument control system (ICS) for interfacing the AO system with the telescope and the users. A VME bus based real time computer, Concurrent 9552-2-R4-P, equipped with double MIPS R4400 CPUs running

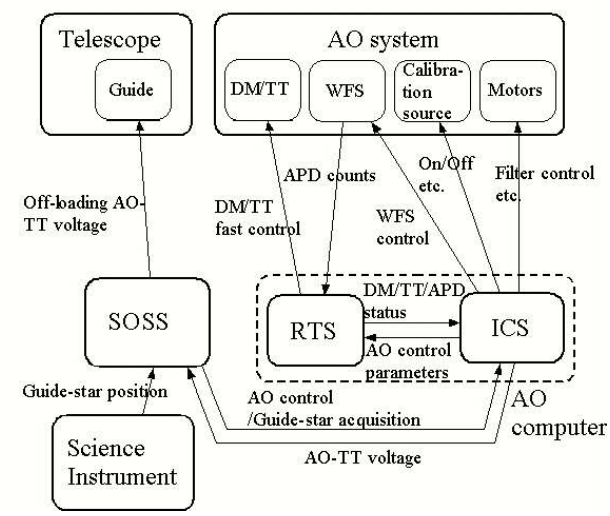

Fig. 12. Control diagram of the Subaru adaptive optics system. The real time control system (RTS) and the instrument control system (ICS) share the control of the AO system. The ICS monitors the voltages applied to the deformable mirror, tip/tilt mirror, and the APD counts and drives the motors of stages and filters in the AO and WFS optics. The SOSS, Subaru Observation Software System, generates commands to control the AO system, the Subaru telescope, and Science instruments. The AO can acquire a guide star using the position information at the science instrument through the SOSS. The SOSS also offloads the angle of tilt of the tip/tilt mirror to the Subaru Telescope guide system.

on MaxOS 4.2 operating system is employed for the real-time control. One of the two CPUs performs the real-time control. The APD counts read by counter boards mounted on the VME bus are processed by this CPU to generate signals issued by the D/A boards to drive the deformable mirror. The second CPU takes care of the communication with the ICS. A maximum control bandwidth wider than 100 Hz is achieved thanks to a wavefront sensor sampling speed of about 2.1 kHz. An example of closed-loop timing is shown in table 3 for a sampling speed of 2.0 kHz. APD counts are read twice in each cycle, in accordance with the focal modulation generated by the vibrating mirror, whereas the updated voltage is applied to the deformable mirror only in the second half of the cycle since the VME bus is not fast enough to finish the voltage update during the first half of the cycle. This arrangement causes a slight delay in response but this is not critical for 2 kHz operation.

Another computer, a SUN Ultra-60 with a SparcII 450 MHz processor and Solaris 2.6 UNIX operating system takes care of the graphical user interface, power supply control, motor control, and other miscellaneous functions. This ICS communicates with the Subaru Observing Software System (SOSS) that supervises the coordinated operation of the telescope and the instrument.

The response matrix used to derive the driving voltage of the 36 electrodes of the deformable mirror from the measured outputs of 36 APDs is fairly diagonal due to optimization of the geometry of the curvature sensor and the deformable mirror. Figure 13 shows the response matrix derived by driving an individual actuator and measuring its response in APD count

Table 3. Timing in the loop software.

Time in loop	Task	Time needed by task
0– 77 μs	read APD counts, compare signal	77 μs
77–167 μs	matrix operation to get DM voltage	90 μs
167–250 μs	wait for next trigger to read	83 μs
250–327 μs	read APD counts	77 μs
327–472 μs	apply voltage to DM	145 μs
472–497 μs	calculate TT voltage and apply to TT	25 μs

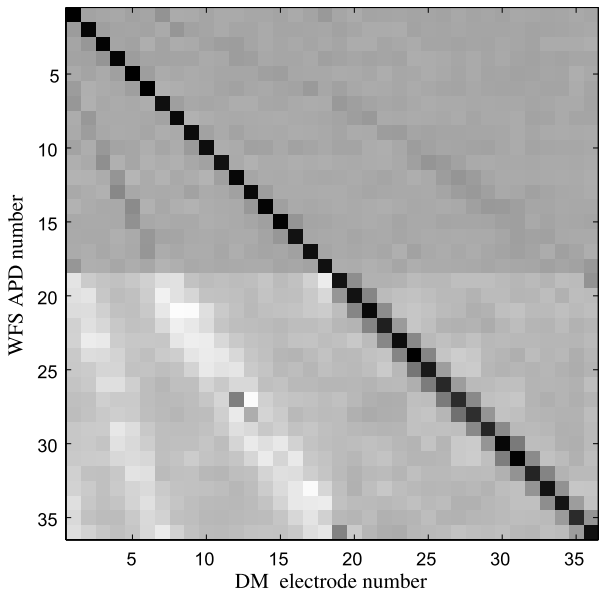

Fig. 13. The diagonal character of the Subaru Cassegrain AO response matrix.

changes. The nearly diagonal-nature of the matrix, as is clear in the figure, is helpful for stable and fast operation of the closed loop servo control. The geometries of the curvature sensor and the bimorph mirror were adjusted elaborately to make this closed-loop response matrix as diagonal as possible.

2.5. *Instruments*

Two science instruments can be operated with this AO system. One is a near-infrared camera/spectrograph (IRCS) with 23 and 58 mas per pixel scale for imaging, spectral resolution R = 640 at K-band for 0.″1 slit in grism mode, and R = 20000 at K-band for 0.″15 slit in echelle mode (Kobayashi et al. 2000; Terada et al. 2003). The other instrument is a coronagraph imager with adaptive optics (CIAO) with 11 and 22 mas per pixel to observe faint objects near a bright sources (Tamura et al. 2000; Murakawa et al. 2003). The direct light from the central bright point source, reduced in size by means of the AO, can be removed by a mask of diameter ranging from 0.″1 to 4.″0 and the remaining scattered/diffracted light is removed by means of another apodizing mask placed in the pupil plane of the instrument. Both instruments cover the 1–5 μm wavelength range with 1 k $\times$ 1 k InSb Aladdin detector. The wavefront sensor, currently shared by these instruments, is directly mounted on the instrument to minimize the mechanical flexure. The beam splitters that divide the light between the instrument and the wavefront sensor are installed inside the cryostats of these instruments. This arrangement is useful for reducing any additional thermal background from the beam splitter.

2.6. *Observing Procedure*

Open-use observers using the AO system should first select the observing targets for which appropriate nearby guide stars are available. The AO guide stars should be $R \leq 18$ and within about 30″ from the observing target object. Using an object broader than 2″ or multiple objects, as a guide star, will increase the wavefront sensing error and lead to deteriorated AO correction performance. The satisfactory AO correction is not achieved under a poor seeing condition, $\geq$ 1.″0, and preparation of backup targets for such an occasion is recommended. Users will be supported by the telescope operator, AO support scientist/operator, and the instrument support scientist/operator. Once a target object is acquired in the FOV of the instrument, the AO support scientist or the operator will optimize the control parameters and close the real-time control loop. If very accurate pointing is required, for example for spectroscopy or for coronagraphic imaging, the fine pointing procedure is conducted by moving the WFS acquisition optics. It is essential to confirm the details of observation with the AO support astronomer and the instrument support astronomer well before an actual run.

3. Verified Performance

3.1. *Preliminary Tests on the Prototype System*

Prior to starting the fabrication of the common-use AO system, a full-size prototype system was constructed. The optical design, deformable mirror, and loop control computer of this system were identical to those of the final Subaru AO system, while the wavefront sensing detectors were less-sensitive analog APDs and the guide star acquisition optics was not installed.

We attached the prototype system to a 1.5 m infrared telescope at the Mitaka campus of NAO, and performed test observations in 1996 September and in 1997 March. An infrared camera equipped with an Amber 256 $\times$ 256 InSb detector with video output was used in combination with an f-conversion optics for the observations. K-band images of α Ori, with and without compensation, were obtained. The FWHM of the compensated image, taken under 2″ seeing at

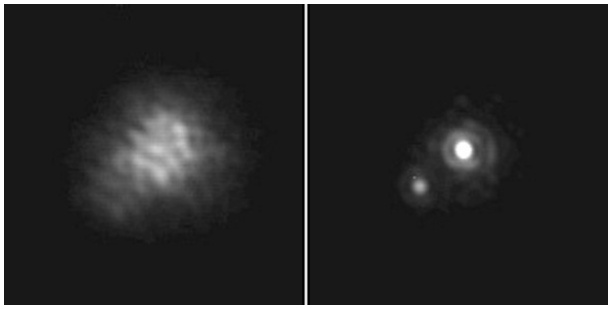

Fig. 14. Binary star HR 1852 imaged with (right) and without (left) an AO correction at the K-band. The separation of the stars is 0.″31.

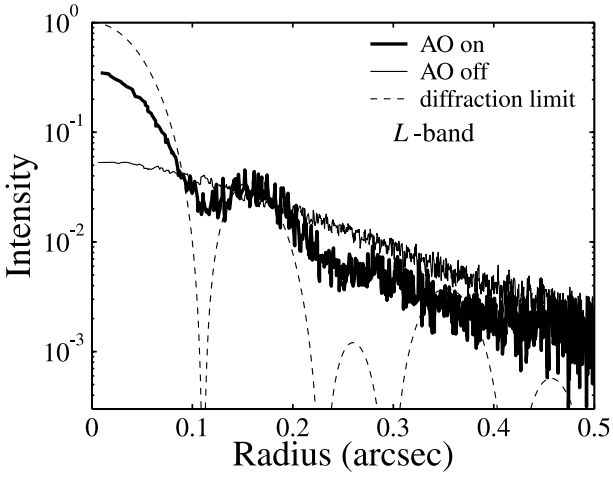

Fig. 15. Point spread functions of AO corrected (thick line), uncorrected (thin line), and the diffraction limited (broken line) stellar images in the L'-band. The FWHMs of corrected and uncorrected images are 0.″1 and 0.″5, respectively.

K-band, was 0.″4, larger than the diffraction limited image size, mainly because the image jitters were not fully compensated at that time. The effective control bandwidth during these observations was about 30 Hz due to incomplete adjustment of the control parameters. However, a factor of improvement in Strehl ratio as high as 20 was achieved at the K-band.

3.2. *Engineering Run*

Based on the various tests performed on the prototype AO system, the current AO system was fabricated entirely newly on a frame to be actually mounted at the Cassegrain focus. The basic design of the new system was copied from the prototype, but the analog mode APD sensors were replaced by those operating in photon-counting mode. Other revisions on various parts were also made.

The entire AO system thus assembled in Japan was transported to the Hilo office of the Subaru observatory in Hawaii in 2000 April. Major reconstruction of the control electronics to fit them in two new electronics racks to be mounted on the telescope was undertaken. Also made were major revisions of the control software to operate the system more easily in conjunction with the available telescope environment (Gaessler et al. 2002). The first light at the Subaru Telescope was

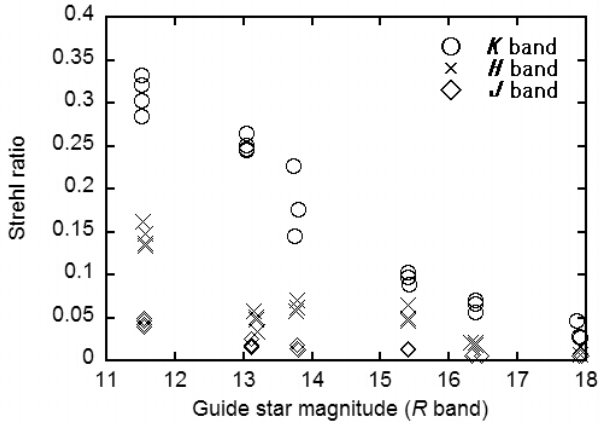

Fig. 16. J, H, K-band Strehl ratio vs. guide star magnitude at R-band under a good seeing condition, 0.″4 at K-band. The Strehl ratio includes the optical aberration effect of the instrument IRCS, which is estimated to give the Strehl ratio better than 0.87 at K-band. The poor performance at the H-band for a 13th magnitude guide star was due to sudden degradation of the seeing at that time. The Strehl ratio without an AO correction was 0.011, 0.0072, and 0.0027 from the K to J-bands.

carried out in 2000 December with IRCS, followed by several engineering runs. Examples of images taken during these runs are shown in figure 14 and figure 15. The corrected image sizes at K-band were 0.″065–0.″07, nearly equal to the diffraction-limited resolution. The results of the engineering runs for verifying the performance of the system are discussed below.

3.3. *Strehl Ratio vs. Guide Star Magnitude*

In order to measure the Strehl ratio at the J, H, and K-bands for guide stars of different magnitude, we changed the neutral-density filter in front of the lenslet array instead of actually changing guide stars. Figure 16 shows the Strehl ratio in the J, H, and K-bands achieved as a function of the effective magnitude of the guide star. We confirmed in previous observations that the Strehl ratio obtained by this method is not different from that obtained with real faint stars. The range of equivalent guide star magnitude covers 11.6 to 17.9 mag at R-band corresponding to average APD counts on a sub-aperture of 125000 to 350 count s^{-1}. The Strehl ratio that we obtained for a bright guide star was 0.31, 0.15, and 0.04 at K, H, and J-bands, respectively, under seeing conditions of 0.″4–0.″5 at K-band during the measurement. We had an improvement of the Strehl ratio by a factor as large as 3, even for an 18th magnitude guide star, with only 350 photon-counts per second per sub-aperture.

Early assessment of the comparison of the measured Strehl ratio to that derived from simulations indicated the presence of a discrepancy. However, by refining the simulation model to include more realistic parameters, the discrepancy now appears to be insignificant. The Strehl ratio measured on the sky was found to be consistent with that expected from simulations within the measurement error of the actual seeing.

The actual statistics of an image size improvement using the current AO system for open-use IRCS observations from 2002 May to 2003 May are shown in figure 17. For observations where a guide star brighter than $R = 12$ mag is available, the

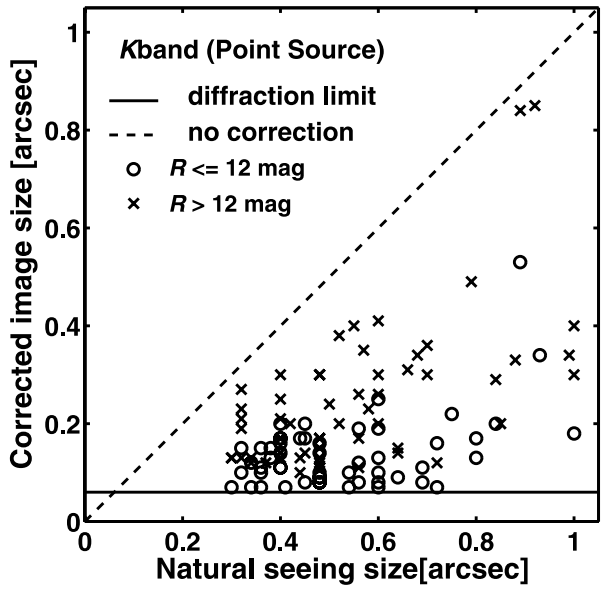

Fig. 17. Actual statistics of the image size improvement for open-use observations using IRCS and the current AO system from 2002 May to 2003 May.

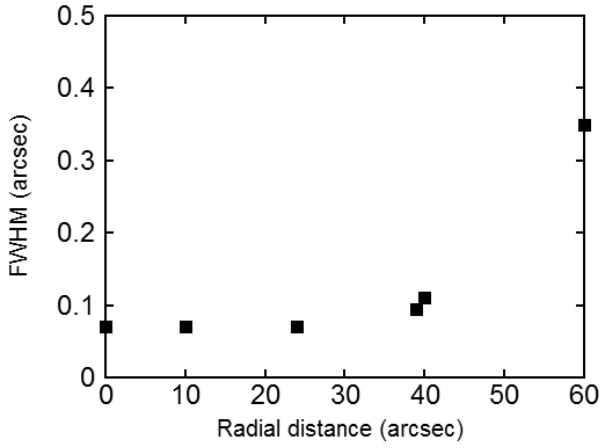

Fig. 18. Variation of image FHWM in the K-band under 0.″55 seeing with distance from the guide star.

image improvement is more significant than for observations where only a fainter guide star is available.

3.4. Isoplanatic Angle

We measured the isoplanatic angle provided by the present system by observing the globular cluster M 15 at the K-band. Figure 18 shows the FWHM degradation as a function of the distance from the guide star. No significant degradation of FWHM was seen up to 24″ from the guide star for a night of observation when the K-band seeing was 0.″5–0.″6. The isoplanatic angle, $\theta_{\rm iso}$, is given by $\theta_{\rm iso} = 0.314\, r_0/h$, where h is the height of the effective turbulent layer and r_0 is the Fried length. Taking the seeing size, $s = 0.''55$ at K-band, the Fried length $r_0 = \lambda/s$ is about 83 cm. Figure 18 suggests that the isoplanatic angle of the night was larger than 30″, and hence the effective height of the turbulent layer was lower than 1.79 km. This is much lower than the assessment of the effective turbulence height of 6.5 km reported by Racine and Ellerbroek (1995). Our result is more consistent with, but still lower than, the height of 3.5 km evaluated at Gemini using the Hokupa'a AO system (Flicker, Rigaut 2002). Actual effective height of the turbulent layer may well be varying from night to night, as well as throughout the night.

Table 4. Optical throughput of the AO system.

Band	Throughput (%)	Background increase (%)
J	88.6 ± 0.3	1.21 ± 34.4
H	91.3 ± 0.4	-2.99 ± 11.2
K'	90.3 ± 0.6	14.4 ± 10.4
K	91.7 ± 0.7	36.3 ± 11.3

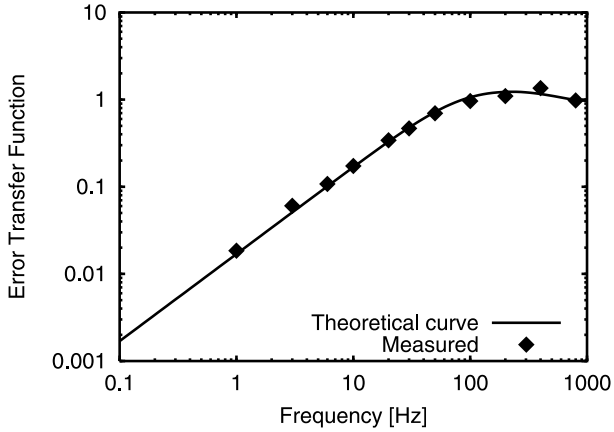

Fig. 19. Measured transfer function for the curvature error of the AO system. The 0 dB bandwidth is 100 Hz for a servo gain of 0.18. The control cycle rate is 2060 Hz. The integration time is 0.49 ms, and the delay from computation and deformable mirror voltage update is 0.39 ms. The solid curve is the theoretical transfer function calculated using the above parameters.

3.5. Dynamic Response

We measured the frequency response of the error suppression rate in the laboratory (figure 19). The correction frequency of the system was 2060 Hz with a servo gain of 0.18. This is consistent with the curve calculated from digital control theory. The effective bandwidth with zero error suppression was 100 Hz.

3.6. Optical Throughput

The optical throughput of the current AO system was measured by observing a star using the camera mode of IRCS with and without AO optics. The derived throughput and the measured increase of the background by inserting the AO optics are given in table 4. The throughput in the infrared bands was verified to be about 90%, consistent with those expected from the calculated reflectivity and throughput of the optical components involved.

3.7. Tip-Tilt Correction

The correction of the tip-tilt wavefront error due to the atmosphere and the telescope tracking error is performed in multiple ways. The paraboloid camera mirror, M5, is tip-tilted with a response time of about 1 sec to cancel the mean tilt of the deformable mirror. This is achieved by a simple integral servo loop. In order to keep the travel of the tip-tilt of the camera mirror within a stroke of ± 2 sec, the accumulated tip-tilt error signal is off-loaded intermittently to the telescope tracking control.

However, it turned out that this caused a non-uniform background illumination that became apparent for long integration observations and for mid infrared L-band observations. This was because the camera mirror was not exactly conjugate to the pupil, and hence tilting the camera mirror made the instrument see different parts of the telescope. Until a fundamental realignment of the system is accomplished, one must alter the telescope pointing instead of tilting the camera mirror to avoid this effect for deep imaging or for L-band imaging. For usual observations, a tip-tilt correction using the paraboloid camera mirror is performed.

4. Laser Guide Star AO System

The sky coverage of the current Subaru AO system based on natural guide stars, despite the high sensitivity of its wavefront sensor, is of the order of 1%, which is not high enough for supporting general common-use AO observations. Finding an appropriate guide star is difficult in high galactic latitude regions, where distant galaxies are often sought. Expanding the sky coverage of the Subaru AO system to nearly the whole sky is extremely important.

Implementing a laser guide star system will remove this difficulty, and a five-year special grant-in-aid for promotion of science was awarded in FY2002 to upgrade the current Cassegrain AO system. The upgrade plan consists of two projects. Increasing the control elements from 36 to 188 by configuring a new AO system with a wavefront sensor with 188 APDs and a new bimorph deformable mirror is one main enterprise under final design study and is foreseen to have its first light in 2005.

Another new initiative is the installation of a sodium layer guide star system (Hayano et al. 2000). A continuous-wave sodium laser with an output power larger than 4 W to generate a laser guide star bright enough for our new AO system is under construction. We are testing a dye laser (Coherent 899) to evaluate its performance. The development of a solid-state laser system is also under way. Plans for installing a laser laboratory above the Nasmyth floor, mounting a laser launching telescope on the Subaru Telescope, and deploying a fiber transmission optics between the laser source and the launching telescope are under investigation.

5. Conclusion

The Cassegrain adaptive optics system, a curvature-sensor based system with 36 control elements, was constructed and has been offered for open-use since 2002 April for observations with IRCS, an infrared camera and spectrograph, or with CIAO, a coronagraph imager with adaptive optics. The Strehl ratio achieved under favorable seeing conditions with natural guide stars $R \leq 12$ is 0.3 at the K-band. The isoplanatic angle measured in one occasion was about $40''$ in radius. The system works well for guide stars as faint as $R = 18$. Plans to upgrade the current system to increase the number of control elements to 188 and to install a sodium laser guide star system are under progress.

We would like to thank all the Subaru Telescope staff for their support to construct, assemble, and test the AO system. Collaborations with IRCS and CIAO team members to verify the performance of the AO system were extremely useful. We acknowledge Dr. M. Watanabe for calculating the theoretical optical throughput of the current AO system.

The early part of the developmental studies of the adaptive optics system was supported by grants-in-aid for scientific research by the Ministry of Education, Culture, Sports, Science and Technology (Project Numbers: 03554002, 04405008, 05305008) and by a grant from the Graduate University for Advanced Studies. A significant fraction of the building cost of the prototype system was supported by the Communications Research Laboratory. The total cost of the Subaru AO system was about 2 million dollar and was part of the construction budget of the Subaru Telescope.

References

Babcock, H. W. 1953, PASP, 65, 229
Bloemhof, E. E., Marsh, K. A., Dekany, R. G., Troy, M., Marshall, J., Oppenheimer, B. R., Hyward, T. L., & Brandl, B. 2000, Proc. SPIE, 4007, 889
Flicker, R. C., & Rigaut, F. J. 2002, PASP, 114, 1006
Gaessler, W., Takami, H., Takato, N., Hayano, Y., Kamata, Y., Saint-Jacques, D., Minowa, Y., & Iye, M. 2002, Proc. SPIE , 4494, 30
Graves, J. E., Northcott, M. J., Roddier, F. J., Roddier, C. A., Potter, D., O'Connor, D. J., Rigaut, F. J., & Chun, M. R., 2000, Proc. SPIE, 4007, 26
Graves, J. E., Roddier, F. J., Northcott, M. J., Anuskiewicz, J., & Monnet, G. 1994, Proc. SPIE, 2201, 502
Hayano, Y., Takami, H., Takato, N., Kanzawa, T., Kamata, Y., Nakashima, K., Iye, M., & Oya, S. 2000, Proc. SPIE, 4007, 149
Iye, M., et al. 2003, PASJ submitted
Kobayashi, N., et al. 2000, Proc. SPIE, 4008, 1056
Miyashita, A., et al. 2003, Proc. SPIE, 4837, 255
Miyazaki, S., et al. 2002, PASJ, 54, 833
Motohara, K., et al. 2002, PASJ, 54, 315
Murakawa, K., et al. 2003, Proc. SPIE, 4841, 881
Otsubo, M., Iye, M., Takami, H., Takato, N., & Hayano, Y. 1995 in Scientific and Engineering Frontiers for 8-10m Telescopes, 1994, ed. M. Iye & T. Nishimura (Tokyo: Universal Academy Press), 333
Otsubo, M., Takami, H., & Iye, M. 1997, PASP, 109, 1057
Racine, R., & Ellerbroek, B. L. 1995, Proc. SPIE, 2534, 248

Roddier, F. 1998, PASP, 110, 837
Roddier, F., Northcott, M., & Graves, J. E. 1991, PASP, 103, 131
Roddier, N., & Roddier, F. 1989, Proc. SPIE, 1114, 92
Takami, H., et al. 2003a, in Masslosing Pulsating Stars and their Circumstellar Matter, ed. Y. Nakada, & M. Honma (Dordrecht: Kluwer ASS Library)
Takami, H., & Iye, M. 1994, Proc. SPIE, 2201, 762
Takami, H., Iye, M., Takato, N., Hayano, Y., & Otsubo, M. 1994, in Scientific and Engineering Frontiers for 8-10m Telescopes, 1994, ed. M. Iye & T. Nishimura (Tokyo: Universal Academy Press), 327
Takami, H., Takato, N., Hayano, Y., Iye, M., Kamata, Y., Minowa, Y., Kanzawa, T., & Gaessler, W. 2003b, Proc. SPIE, 4839, 21
Takami, H., Takato, N., Kanzawa, T., Hayano, Y., Kamata, Y., Gaessler, W., Minowa, Y., & Iye, M. 2001, ed. E. Vernet, R. Raggazoni, S. Esposito, & N. Hubin, ESO Conference and Workshop Proc., 58, 427
Takami, H., Takato, N., Otsubo, M., Kanzawa, T., Kamata, Y., Nakashima, K., & Iye, M. 1998, Proc. SPIE, 3353, 500
Takato, N., Iye, M., & Yamaguchi, I. 1994, PASP, 106, 182
Tamura, M., et al. 2000, Proc. SPIE, 4008, 1153
Terada, H., et al. 2003, Proc. SPIE, 4841, 1306